Available online at www.sciencedirect.com
ScienceDirect
Advances in Space Research 42 (2008) 1527–1537
ADVANCES IN SPACE RESEARCH (a COSPAR publication)
www.elsevier.com/locate/asr

Results from the ESA SREM monitors and comparison with existing radiation belt models

H.D.R. Evans [a,b,*], P. Bühler [c], W. Hajdas [d], E.J. Daly [a], P. Nieminen [a], A. Mohammadzadeh [a]

[a] European Space Agency, ESTEC, Postbus 299, Noordwijk, 2200 AG, The Netherlands
[b] Rhea System SA, B-1348 Louvain-la-Neuve, Belgium
[c] PB, AT-1130, Vienna, Austria
[d] Paul Scherrer Institut, CH-5232 Villigen PSI, Switzerland

Received 1 November 2006; received in revised form 4 March 2008; accepted 19 March 2008

Abstract

The Standard Radiation Environment Monitor (SREM) is a simple particle detector developed for wide application on ESA satellites. It measures high-energy protons and electrons of the space environment with a 20° angular resolution and limited spectral information. Of the ten SREMs that have been manufactured, four have so far flown. The first model on STRV-1c functioned well until an early spacecraft failure. The other three are on-board, the ESA spacecraft INTEGRAL, ROSETTA and PROBA-1. Another model is flying on GIOVE-B, launched in April 2008 with three L-2 science missions to follow: both Herschel and Planck in 2008, and GAIA in 2011). The diverse orbits of these spacecraft and the common calibration of the monitors provides a unique dataset covering a wide range of B-L* space, providing a direct comparison of the radiation levels in the belts at different locations, and the effects of geomagnetic shielding. Data from the PROBA/SREM and INTEGRAL/IREM are compared with existing radiation belt models.

Keywords: Radiation monitor; Radiation environment; SREM; Radiation belt model; AE-8; AP-8; Solar proton events; Magnetosphere

1. SREM instrument

The SREM consists of three detectors (D1, D2, and D3) in two detector head configurations. One system is a single silicon diode detector (D3). The main entrance of the D3 window is covered with 0.7 mm aluminum, which defines the lower energy threshold for electrons to ~0.5 MeV and for protons to ~10 MeV. The other system uses two silicon diodes (detectors D1/D2) arranged in a telescope configuration. The main entrance of this detector is covered with 2 mm aluminum giving a proton and electron threshold of 20 and 1.5 MeV, respectively. A 1.7-mm-thick aluminum and 0.7 mm thick tantalum layer separate the two diodes of the telescope configuration.

The telescope detector allows measurement of the high-energy proton fluxes with enhanced energy resolution. In addition, the shielding between the two diodes in the telescope prevents the passage of electrons. However, protons with energies greater than 43 MeV go through. Thus, using the two diodes in coincidence gives pure proton count rates allowing subtraction of the proton contribution from the electron channels. A total of 15 discriminator levels are available to bin the energy of the detected events. Any two of the levels can be used to raise an alarm flag when the count rates exceed a programmable threshold. This alarm signal can then be used to control the operation of the spacecraft and its instruments. The detector electronics is capable of processing a detection rate of 100 kHz with dead-time correction below 20%.

The SREM is contained in a single box of $20 \times 12 \times 10\ \text{cm}^3$ and weighs 2.6 kg, see Fig. 1. The box contains the detector systems with the analog and digital

* Corresponding author. Address: European Space Agency, ESTEC, Postbus 299, Noordwijk, 2200 AG, The Netherlands.
E-mail address: Hugh.Evans@esa.int (H.D.R. Evans).

0273-1177/$34.00 © 2008 COSPAR. Published by Elsevier Ltd. All rights reserved.
doi:10.1016/j.asr.2008.03.022

Fig. 1. Picture of SREM flight model.

front-end electronics, a power supply, and a TTC-B-01 Telemetry and Telecommand interface protocol. By virtue of a modular buildup, the interface can be adapted to any spacecraft system. The power consumption is approximately 2.5 W. An essential input for the interpretation of the detection rates, in terms of particle fluxes, are the energy dependent response functions. Therefore, prior to launch, the instruments are fully calibrated at the Proton Irradiation Facility, (PIF) of Paul Scherrer Institut (PSI) (Hajdas et al., 1996). In addition, the instrument and the host spacecraft are simulated with the Geometry and Tracking (GEANT) 3.21 and GEANT4 particle transport codes to accurately determine the response functions to electrons at energies between 0.3 and 15 MeV and to protons in the 8–800-MeV range.

In addition to 15 energy bins, three counters are assigned to detector one to three dead-time correction values, respectively. Table 1 lists all SREM counters.

As explained earlier, the D1/D2 configuration measures protons from approximately 20 MeV to infinity. Events detected by this configuration are divided into 10 bins, (including four proton coincidence bins) and one heavy ion bin. SREM is incapable of discriminating between various heavy ion particle types and identifies particles as heavy ions, in one bin only, if their deposited energy in D2 is higher than 9 MeV. The D3 sensor is sensitive to electrons with energies from 0.5 MeV, and is also sensitive to protons, requiring that a deconvolution procedure must be applied to obtain particle spectra in mixed environments. In addition to the D1–D3 particle counters, the SREM includes an internal RADFet and capacity to connect up to three external RADFets for total dose measurements.

The SREM flying on the INTEGRAL spacecraft has been adapted from the standard SREM configuration, and is hence referred to as the INTEGRAL/IREM.

2. Calibration activities

The calibration of the instruments so as to provide a conversion of raw instrument count rates to particle fluxes is essential. From the fluxes it is possible to obtain derived parameters, such as dose and solar cell degradation, as well as further data analysis and comparison with other instrument models. Calibration activities included both measurements with a beam or a source and software simulations. The source measurements provide both a validation of the software simulation as well as a measurement of the active area of the detector diode. The software simulations are required as it is not possible to irradiate the detector in the flight configuration with the spacecraft shielding geometry and omni-directional particle source.

Each SREM flight instrument has undergone individual irradiation tests with a Sr90 source, Co60 source and at various energies from 12.5 to 100 MeV at the PSI Proton Irradiation Facility. The dead-time measurement of the instruments was performed during the PIF irradiations,

Table 1
List of the SREM counters and the corresponding energy ranges of protons and electrons detected

Bin	Logic	Discriminator level	Proton energy (MeV)			Electron energy (MeV)		
		$\Delta E > XX$ (MeV)	Min (MeV)	Max (MeV)	SCF [#/cm^2]	Min (MeV)	Max (MeV)	SCF (#/cm^2)
TC1	D1	0.085	27	∞	15.8	2.0	∞	118
S12	D1	0.25	26	∞	19.0	2.08	∞	195
S13	D1	0.6	27	∞	16.0	2.23	∞	519
S14	D1	2.0	24	542	38.5	3.2	∞	25403
S15	D1	3.0	23	434	65.6	8.18	∞	5460
TC2	D2	0.085	49	∞	13.1	2.8	∞	191
S25	D2	9.0	48	270	208.8	n/a	n/a	
C1	D1 × D2	0.6, 2.0	43	86	107.22	n/a	n/a	
C2	D1 × D2	0.6, 1.1–2.0	52	278	75.6	n/a	n/a	
C3	D1 × D2	0.6, 0.6–1.1	76	450	35.1	n/a	n/a	
C4	D1 × D2	0.085–0.6, 0.085–0.6	164	∞	10.4	8.10	∞	155
TC3	D3	0.085	12	∞	49.3	0.8	∞	101
S32	D3	0.25	12	∞	49.3	0.75	∞	189
S33	D3	0.75	12	∞	40.2	1.05	∞	1162
S34	D3	2.0	12	∞	63.8	2.08	∞	93077

Also the simple conversion factors (SCF) for the IREM instrument are provided for protons and electrons. The greyed boxes indicate channels that are proton only, and not sensitive to electrons. "n/a" indicates that the SCF column is undefined (not applicable) for this channel.

and it was found that the corrections are linear with flux up to count rates of 50 and 100 k/s for the D1/D3 and D2 detectors, respectively. Recently the SREM EQM has been irradiated with a Sr90 source at the QinetiQ Realistic Electron Environment Facility.

Monte Carlo simulations of the SREM response were performed using CERN code GEANT3 and later also GEANT4. First a detailed mass and geometry computer model of SREM is constructed, consisting of several hundred of components. For comparison with proton and electron calibrations the simulations were carried out for exactly the same energies as in the experimental case and with sufficient statistics. Angular position of the SREM was also taken into account to cover the whole set of proton incidence angles. Detector areas were first re-measured during the experiment and their values were set for simulations. Separate computations were done to find out the fluence at the positions of the detectors heads as well as at the beam centre in order to assure the same conditions as in the experiment. By these means, the correctness of computational setup could be verified and SREM counters values normalized properly. The difference between experimental data and simulation results is within 20% to 30%. Similar comparisons are underway for the REEF irradiations with the Geant4 mass model.

From the Geant4 mass models of the instruments with their associated spacecraft geometries, response functions of the SREM channels to omni-directional fluxes have been derived and the sensitivity of the channels to particle species characterized. These response functions are available from the PSI/SREM website (PSI/SREM).

Several counts to flux conversion methods have been considered: simple conversion factor, an iterative conversion factor and a step function fit. The simple conversion factor (SCF) is based on the mean of the integral transform of the response function with a sampling of space environment spectra; these SCFs for protons and electrons are provided in Table 1. This can provide a first estimate of the flux from the count rate, and in the case of solar proton events, provides reasonable results. The iterative method is an extension of the SCF, where the initial SCF is used to estimate the spectral hardness which is then used to better estimate the SCF. This process is repeated until the flux between steps converges. The step function fit consists of fitting the data channels from SREM to a predefined set of energy bins on a point by point basis. This results in a series of linear equations that relate the counts with the flux levels, which must be inverted to obtain the fluxes. While this method is independent of assumptions over spectral form and hardness, the algebraic solution of the matrix inversion is not trivial and requires a careful approach – if the counts are strongly correlated then the inversion can become unstable.

3. INTEGRAL/IREM data from solar proton events

On the 26th October, 2003 a large coronal mass ejection from the sun occurred, resulting in one of the largest solar proton events of the current solar cycle, with the >10 MeV proton fluxes remaining above the cosmic ray background levels for more than 10 days. The event is composed of several flux enhancements, with the largest, a prompt event,

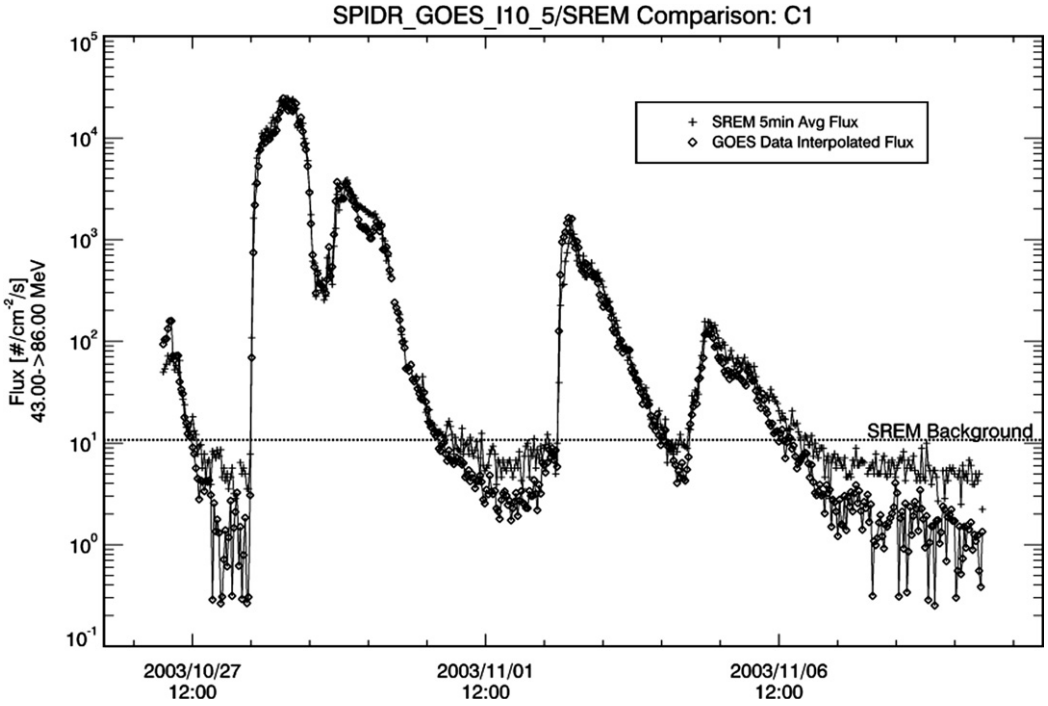

Fig. 2. The SREM/C1 channel (+) scaled by the simple conversion calibration factor over-plotted with the GOES-10 (diamond) integral proton data. The GOES data has been interpolated with a power-law function to the energy range of the SREM/C1 channel.

occurring at mid-day on the 28th and subsequent events in the following days, see Fig. 2.

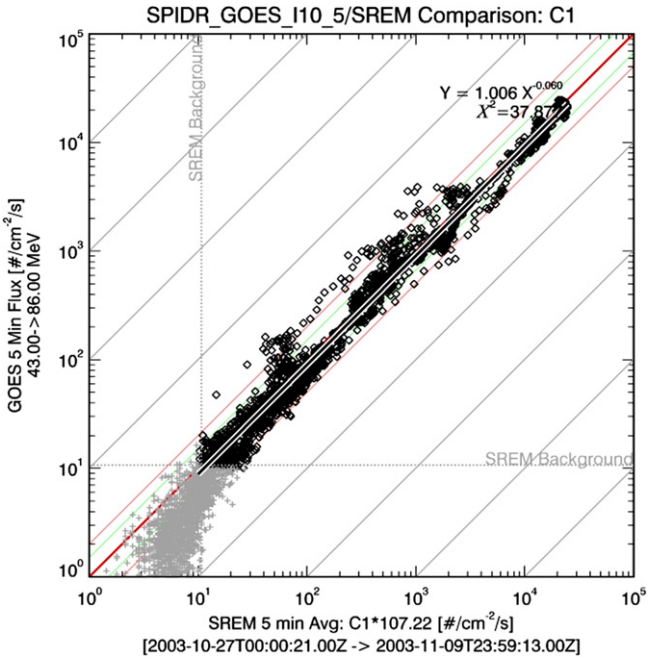

Fig. 3. A scatter plot of the SREM/C1 channel with the power-law interpolated GOES-10 integral data.

The IREM count rates were scaled by the SCFs provided above and compared with a power-law interpolation of the GOES-10 and GOES-11 data available on-line from the NGDC–SPIDR system (NGDC/SPIDR). Even with this simplified conversion factor the IREM data compares within a factor of 2 with the GOES data, with only a few discrepancies that are due to either anisotropies in the flux or geomagnetic shielding, see Fig. 3. At the highest count rates, the data is within a factor of 1.5 of the GOES data and the fit of the data made with fluxes above the estimated background (10 p^+ cm^{-2} s^{-1}) is very good.

The unique positioning of the INTEGRAL (INTEGRAL) and PROBA (PROBA) satellites also permits the investigation of the effects of geomagnetic shielding during solar proton events, as seen in Fig. 4. In the period covered by this plot INTEGRAL was on open magnetic field lines, while PROBA, in low Earth orbit, crossed areas of geomagnetic shielding repeatedly. It can be seen that the onset of the geomagnetic shielding for the higher energy protons (C2, > 52 MeV) appears later in the orbit than the low energy protons (S14, > 12 MeV).

Since Rosetta (ROSETTA) was launched, there have been three significantly large solar proton events, providing an opportunity to compare the interplanetary fluxes measured by Rosetta/SREM with those measured by INTEGRAL/IREM. During the first event in November 2004, Rosetta was leading the Earth, and was poorly connected

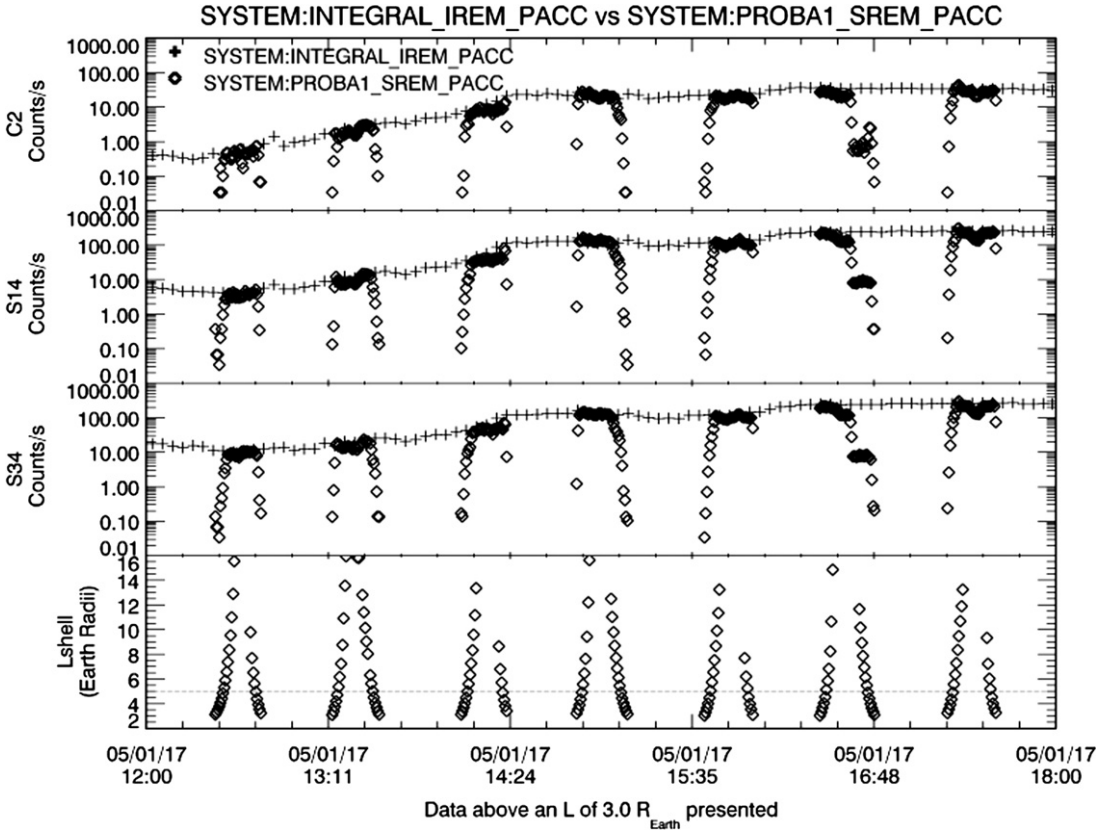

Fig. 4. The S33, S14, and C2 channels from INTEGRAL (+) and PROBA (diamond) during the January 2005 solar proton event. The McIlwain L-Shell parameter for PROBA is plotted in the bottom panel.

to the source of the event. This poor connection, in comparison to the terrestrial connection, resulted in a very different time series of counts from the Rosetta/SREM to the INTEGRAL/IREM, as seen in Fig. 5. The initial event early on the 7th of November is not registered at Rosetta, and the subsequent event on the 9th is entirely different from that measured by INTEGRAL/IREM.

During the event in January 2005, Rosetta was at nearly the same helio-longitude as the Earth and helio-radius and so its connection to the source of the event was very similar to that of INTEGRAL. The time series from the two spacecraft are nearly identical, with the arrival of fluxes at the spacecrafts at the same time, see Fig. 6. There is a slight delay at Rosetta in the rapid decrease of fluxes on the 21st.

In September 2005, another event occurred when Rosetta was trailing the Earth, resulting in a significantly higher fluence of particles at Rosetta than at INTEGRAL. As for the event the preceding year, the time series of the two fluxes are considerably different, with Rosetta seeing a more prompt event than INTEGRAL, and the only distinguishable similarities between the two sets of measurements are the initial gradual rising phase and that the period included two events, see Fig. 7.

4. Magnetospheric missions and radiation belt model comparisons

Two SREMs are currently active and returning data on the Earth's radiation belts. The first is on-board PROBA, which was launched on 22nd October, 2001 into an elliptical sun synchronous orbit with and inclination of 97.9° and a period of approximately 97 min. The path of PROBA covers the polar horns as well as the South Atlantic anomaly and is exposed to energetic particles from the Sun during solar proton events. The second is on-board

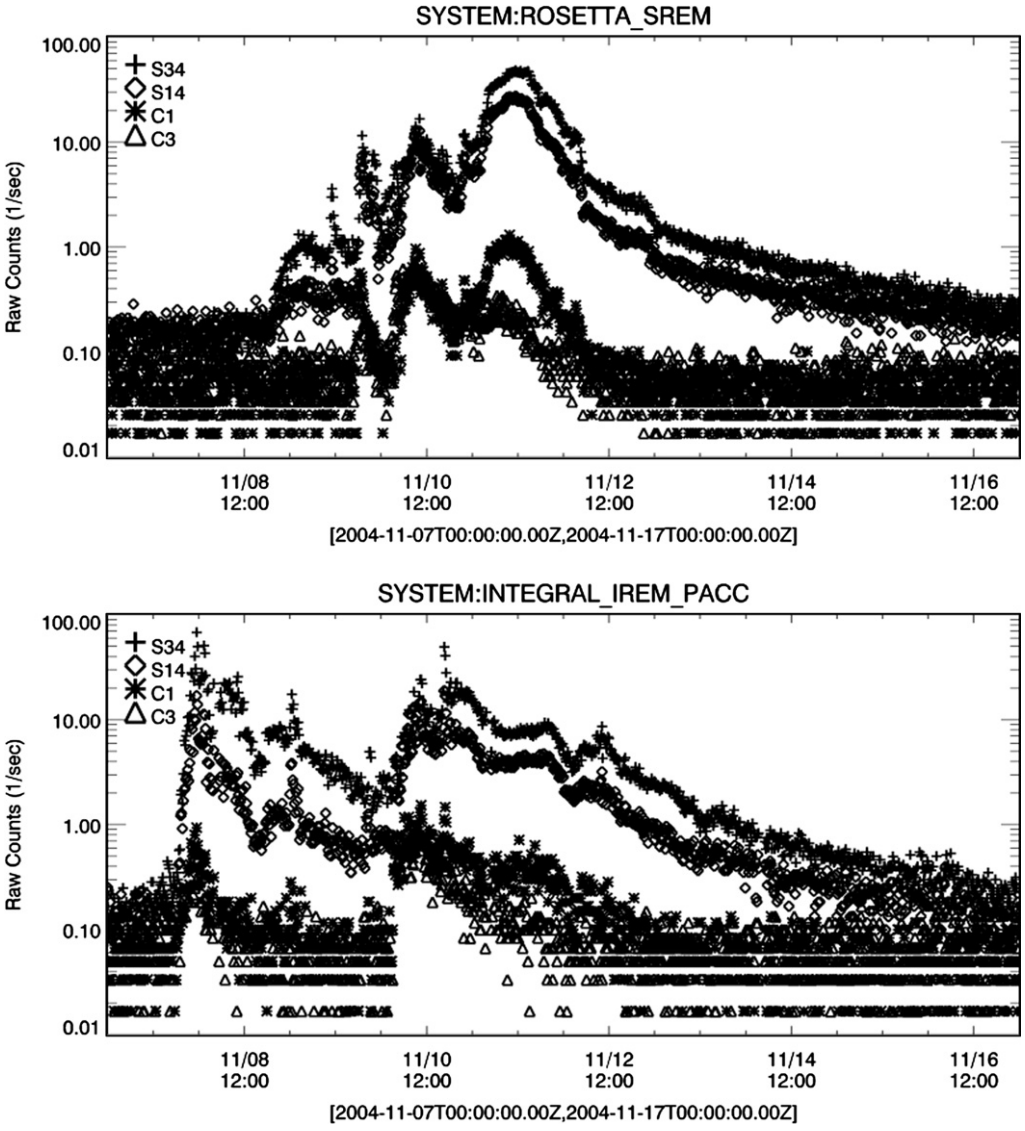

Fig. 5. The Rosetta (upper panel) and INTEGRAL (lower panel) data from the November 2004 solar proton event. The radiation belt passages have been removed from the INTEGRAL data set.

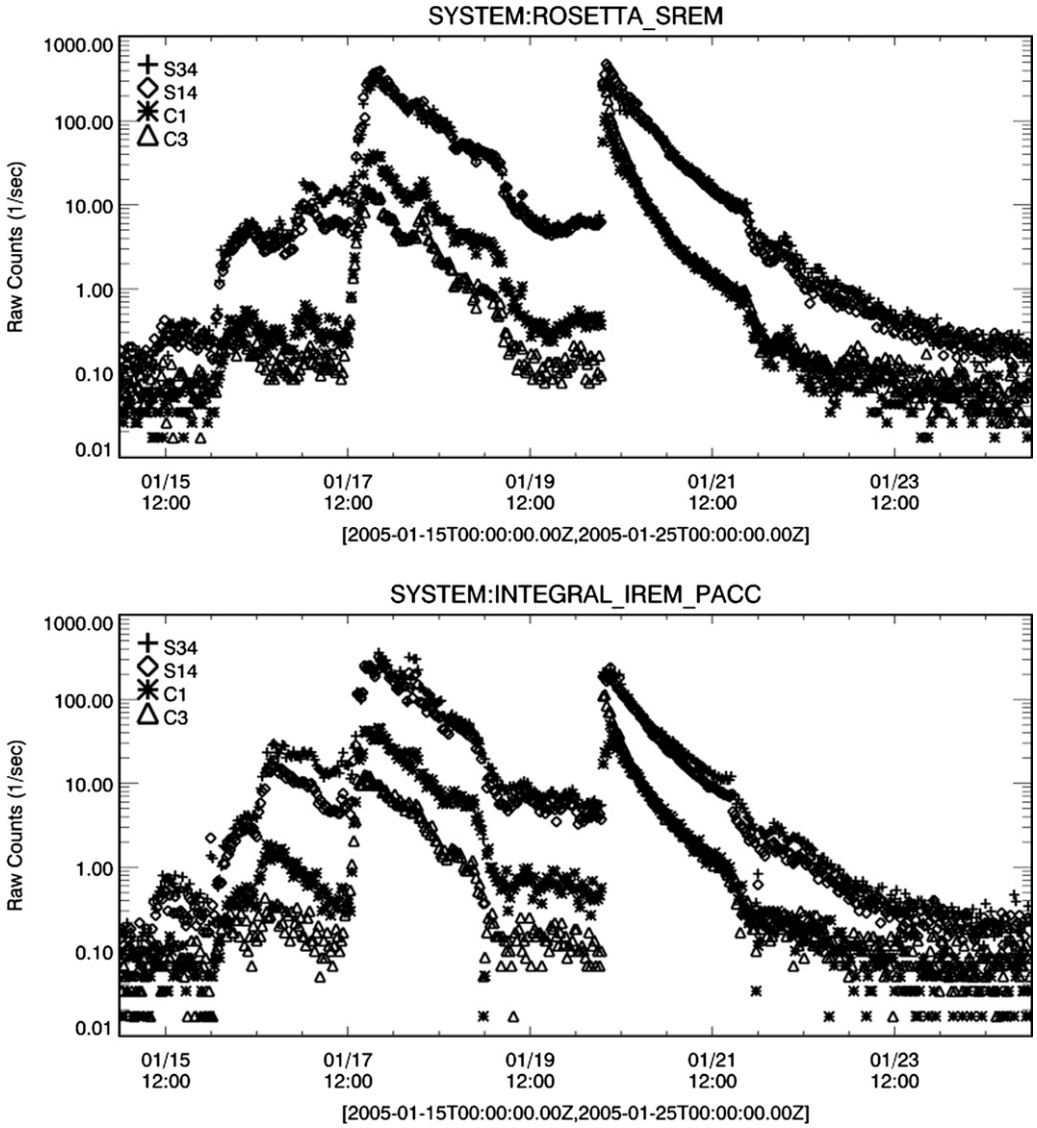

Fig. 6. The Rosetta (upper panel) and INTEGRAL (lower panel) data from the January 2005 solar proton event. The radiation belt passages have been removed from the INTEGRAL data set.

INTEGRAL, which was launched on the 17th October, 2002 into a highly eccentric 72-h period orbit with a perigee of 9000 km, an apogee of 155,000 km and an inclination of 51.6°. The INTEGRAL orbit provides a snap-shot of the fluxes at higher altitudes in the radiation belts every 3 days. The two missions cover a wide range of B-L^* space, as seen in Fig. 8.

Both instruments have collected data during the declining phase of the current solar cycle, and measured the enhancement and decay of the electron fluxes in the highly variable outer belt. Fig. 9 shows the variability of the belts as measured by the two SREMs during the period starting 2003 through to mid 2006. At the beginning of this period, the fluxes in the belts were at high levels, with the heart of the belt located around a Roederer L^* of 4–4.5. The fluxes in the belt slowly decay with the heart of the belt rising to an L^* of about 5 and almost disappearing by June 2004. Subsequently in the following August a large injection event occurred, increasing the intensity of the fluxes to the highest levels of the period.

The recent effects of the coronal hole on the outer electron belt have also been measured by the SREMs, and the data from PROBA is seen in Fig. 10. The repeating 28 day cycle is apparent in the enhancement of the belts, with the heart of the belt extending down to an L^* of 4.2 until the largest enhancement in April 2006 with the heart of the belt extending down to an L^* of 3–3.5.

To compare the results from the two detectors with the various models of the radiation belts requires that the count rates from the instruments are converted to fluxes, or the particle spectra from the models are folded with the response functions of the instrument channels to provided model count rates. For validation of the models, the latter is the preferred choice, as it minimizes the errors inherent in the calibration process and provides the contributions to the total model count rate for the different par-

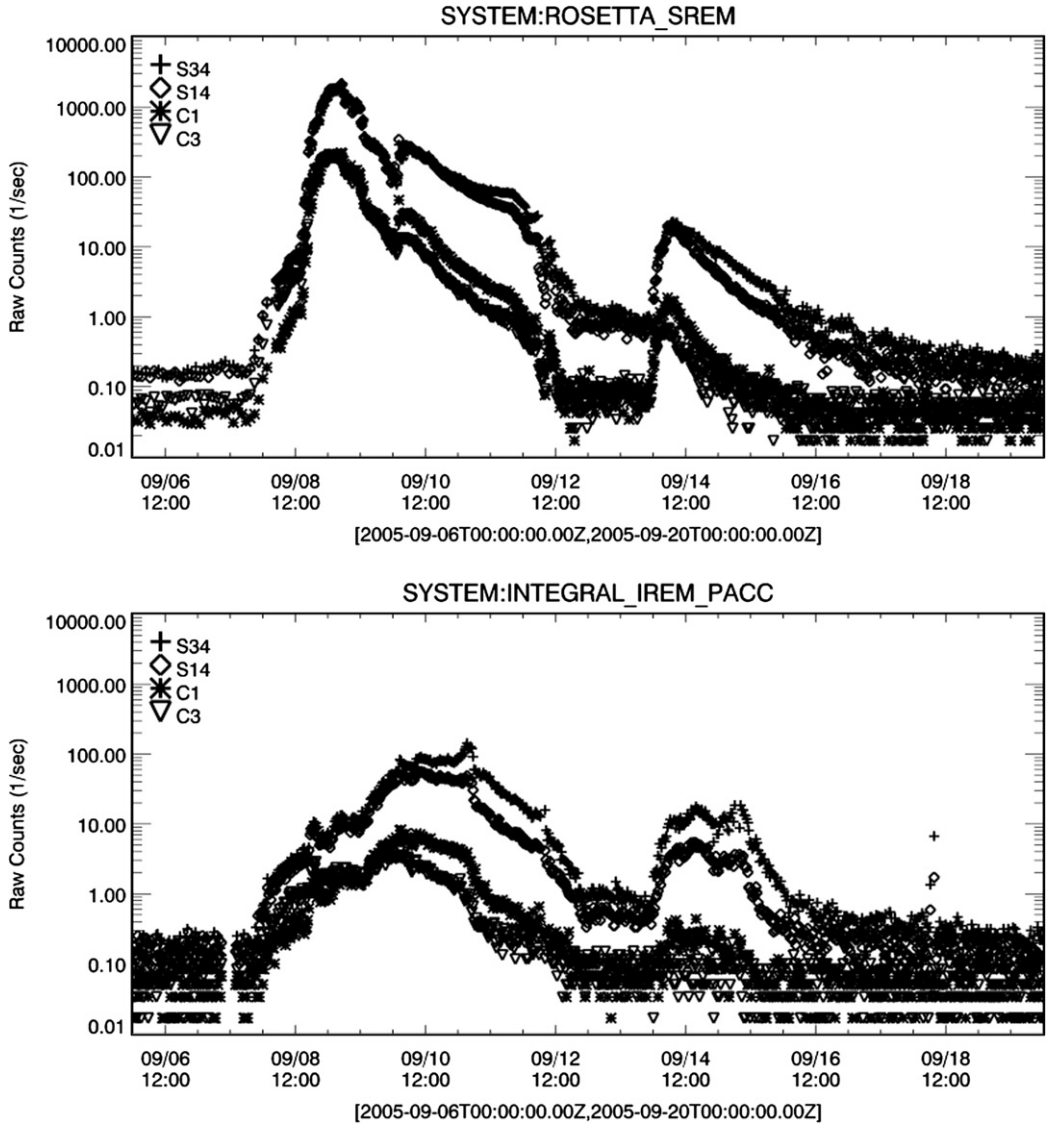

Fig. 7. The Rosetta (upper panel) and INTEGRAL (lower panel) data from the September 2005 solar proton event. The radiation belt passages have been removed from the INTEGRAL data set.

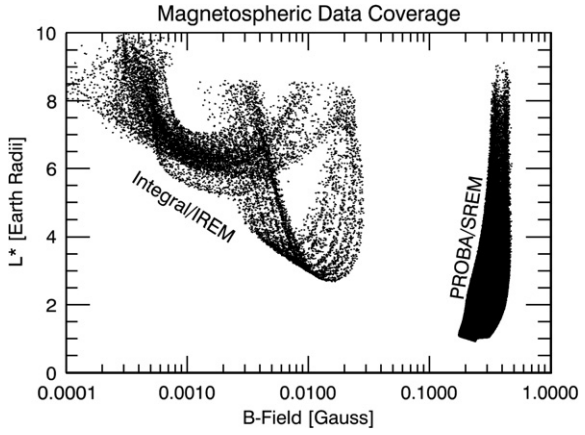

Fig. 8. The coverage of the INTEGRAL and PROBA SREM data in B-L^* space.

ticle species, making it unnecessary to de-convolve the count rates into particle species. This method mimics the approach in which the radiation belt models are used to obtain, for example, mission doses from the omni-directional fluxes provided by the models.

The data has been plotted using the Roederer L^* parameter as calculated using the ONERA/DESP library (ONERA/DESP) from the spacecraft's geographic location with the IGRF model at the data's epoch and the Olson–Pfitzer quiet model (Olson and Pfitzer, 1977). While the McIlwain L-Shell parameter is used as a parameter in the NASA models, the L^* parameter can prove better at organizing multiple datasets and is preferred for model building activities.

The count rates derived from the AE8 and AP8 models were calculated from the geographic location of the spacecraft with the appropriate field model for the model: AP8MIN, AE8MAX and AE8MIN from the Jensen & Cain (Jensen and Cain, 1962) model; and AP8MAX from the GSFC 12/66 model (Cain et al., 1967) extrapolated to 1970.

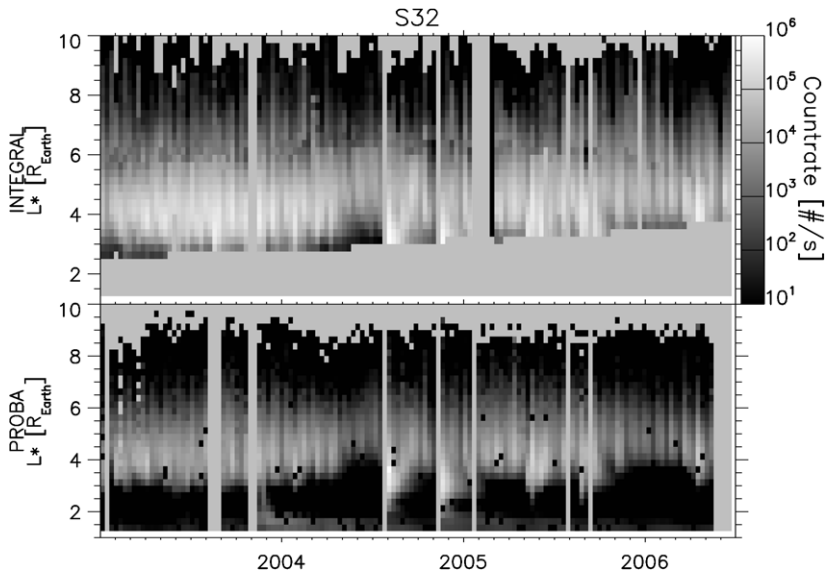

Fig. 9. The S32 channel from the INTEGRAL (upper) and PROBA (lower) SREMs have been binned by 0.2 R_{Earth} L^* by 3 day bins and plotted with a logarithmic grey scale. The asymmetric passage of INTEGRAL through the radiation belts results in the discontinuity seen at an L^* between 5.5 and 6.5.

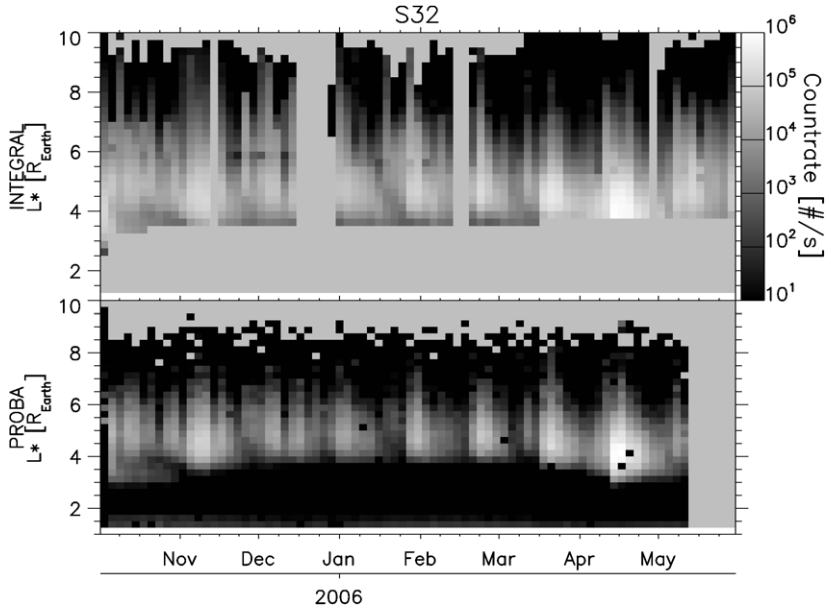

Fig. 10. This figure shows the enhancements to the outer radiation belt as a result of the fast solar wind speeds on the terrestrial magnetic field from a coronal hole.

4.1. INTEGRAL data compared with models

The IREM data between January 2003 and May 2006 from INTEGRAL have been compared with the count rates provided by the following model combinations: AP8MAX/AE8MAX (Vette, 1991), and AP8MIN/AE8MIN (Vette, 1991). For INTEGRAL/IREM, it is the trapped electron belts that dominate the radiation environment.

In Fig. 11 the mean count rates as a function of L^* for the INTEGRAL TC3 channel, corresponding to electron energies >800 keV, are presented with the corresponding mean count rates provided by the radiation belt models. There is very good agreement between the mean of the SREM data and the AE8/AP8 models above an L^* of 5. At the geostationary location of L^*-6.5 to L^*-7, the models prove to be conservative by about a factor of 2. Below an L^* of 5, both of the average models are below the SREM mean, but the AE8MAX/AP8MAX models remain within a factor of 2 of the data, while the AE8MIN/AP8MIN diverges significantly from the data.

Similarly, in Fig. 12 the mean count rates as a function of L^* for the INTEGRAL TC1 channel, corresponding to electron energies >2 MeV, are presented with the corresponding mean count rates provided by the radiation belt models. As with the TC3 channel, the comparison with

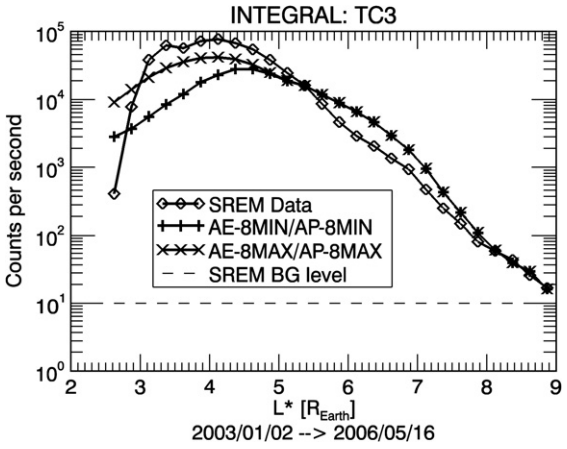

Fig. 11. The mean of the INTEGRAL IREM TC3 count rates (diamond) have been plotted as binned by Roederer L^*. Also shown are the mean count rates of the bins provided from the AE-8MIN/AP-8MIN (+) and AE-8MAX/AP-8MAX (×) models.

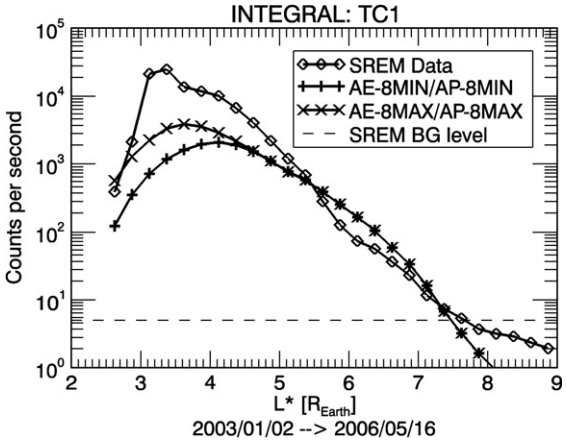

Fig. 12. The mean of the INTEGRAL IREM TC1 count rates (diamond) have been plotted as binned by Roederer L^*. Also shown are the mean count rates of the bins provided from the AE-8MIN/AP-8MIN (+) and AE-8MAX/AP-8MAX (×) models.

the radiation belt models is reasonable above an L^* of 5 and the count rates from the models are within a factor of 1.5–2 of the data. There is a strong divergence between the models and the data below an L of 4.5, with the mean count rates over these L^* up to a factor of 5 or 6 higher than the AE8MAX count rates. The mean of the data for L^* below 4 R_{Earth}, though, is significantly affected by the large event in August 2004, where the peak of the radiation belt was located around an L^* of 3.5 R_{Earth} and the fluxes increased by several orders of magnitude. The rise in perigee of the spacecraft also results in a truncated dataset for that region, see Fig. 9, resulting in a possible over-emphasis of this event.

The results for the TC2 channel, corresponding to electron energies >2.8 MeV, are similar to that from the TC1 channel, see Fig. 13. The models are in reasonable agreement with the data above an L^* of 5 and diverge for lower L^*.

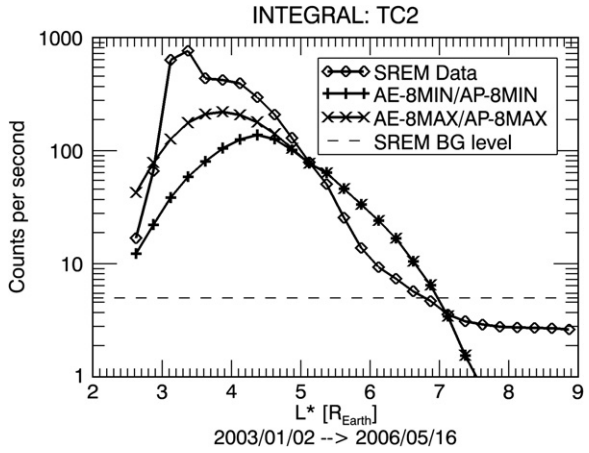

Fig. 13. The mean of the INTEGRAL IREM TC2 count rates (diamond) have been plotted as binned by Roederer L^*. Also shown are the mean count rates of the bins provided from the AE-8MIN/AP-8MIN (+) and AE-8MAX/AP-8MAX (×) models.

4.2. PROBA data comparison with models

The SREM data between October 2001 and May 2006 from PROBA have been compared with the count rates provided by the following model combinations: AP8MAX/AE8MAX (Vette, 1991) and AP8MIN/AE8MIN (Vette, 1991). For PROBA the dominant particle species that affects the count rate is dependent on the channel's susceptibility to the particle and the L^*. In addition, the particles encountered by PROBA, especially in the trapped proton belt, are near their mirror point with a pitch angle near 90°. However, the radiation belt models provide omni-directional fluxes and the instrument response function requires an omni-directional flux spectrum, the integration of the two to provide the model count rate is consistent and this method of comparing the data with the models is generally valid. In this analysis we have selected SREM channels that are not susceptible to electron contamination: S34, S14, and C2, corresponding to energies greater than 12, 24, and 52 MeV, respectively.

In Figs. 14 and 15, the mean count rates for the S34 and S14 raw count rates are plotted with the corresponding mean count rates provided by the AP8MIN and AP8MAX models – the counts from the respective electron models have been included but have no demonstrable significance to the model count rates. Count rates below a background level of 0.4 counts per second were excluded from the data binning. The minor electron contamination for these channels can be seen for L^* above 2.5 R_{Earth}. The count rates from the AP8MAX model, the relevant model for the epoch of the data, is in good agreement overall but exceed the SREM count rates, indicating a general level of pessimism in the model that does exceed a factor of 1.5 for the peak fluxes.

The higher energy coincidence channels, though, do not agree well with the long-term mean count rates provided by the models, as seen in Fig. 16 for the C2 channel. It is suspected that the higher angular fidelity of these coincidence

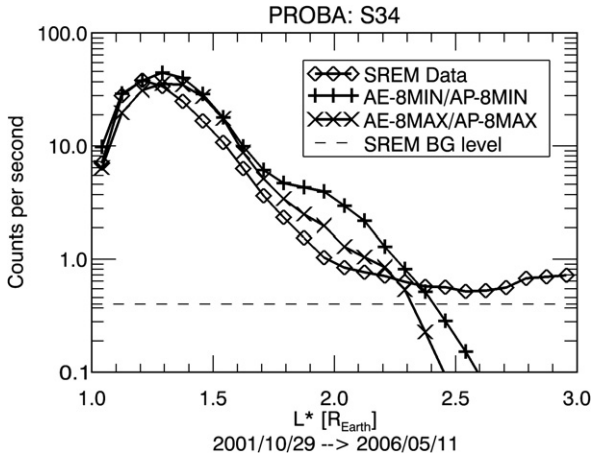

Fig. 14. The mean of the PROBA SREM S34 count rates (diamond) have been plotted as binned by Roederer L^*. Also shown are the mean count rates of the bins provided from the AE-8MIN/AP-8MIN (+) and AE-8MAX/AP-8MAX (×) models.

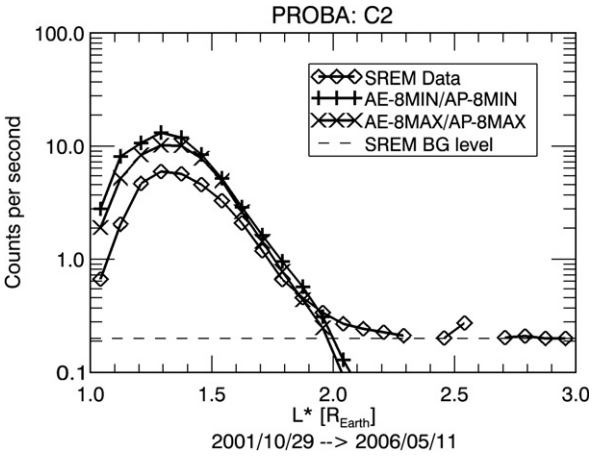

Fig. 16. The mean of the PROBA SREM C2 count rates (diamond) have been plotted as binned by Roederer L^*. Also shown are the mean count rates of the bins provided from the AE-8MIN/AP-8MIN (+) and AE-8MAX/AP-8MAX (×) models.

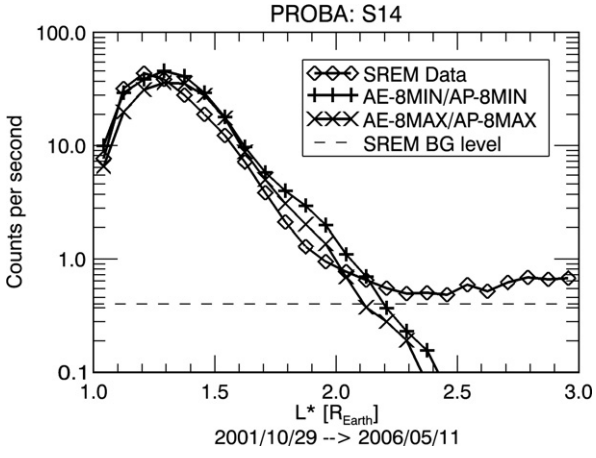

Fig. 15. The mean of the PROBA SREM S14 count rates (diamond) have been plotted as binned by Roederer L^*. Also shown are the mean count rates of the bins provided from the AE-8MIN/AP-8MIN (+) and AE-8MAX/AP-8MAX (×) models.

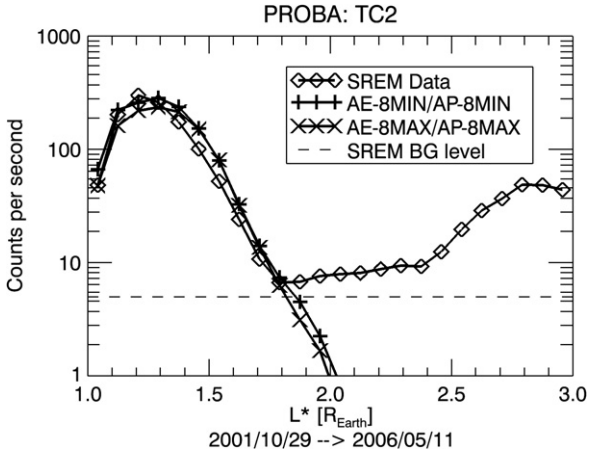

Fig. 17. The mean of the PROBA SREM TC2 count rates (diamond) have been plotted as binned by Roederer L^*. Also shown are the mean count rates of the bins provided from the AE-8MIN/AP-8MIN (+) and AE-8MAX/AP-8MAX (×) models.

channels results in a much stronger pitch angle effect and subsequently lower count rates. The data shown in Fig. 17 from the TC2 channel, which is sensitive to protons with energy above 50 MeV, and is comparable in energy range to the C2 channel, shows very good agreement with the count rates from the models. Additionally, there are radiation belt passages, during which the detector opening scanned the pitch angle distribution, where the correlation of the pitch angle and the coincidence count rates are demonstrated and the relative independence of the non-coincidence count rates with the pitch angle, see Fig. 18. The on-board magnetometers were used to derive the pitch angle of the instrument look direction.

5. Summary

The SREM instruments on PROBA, INTEGRAL and Rosetta are providing a valuable set of data that covers both the near-Earth trapped particle belts and interplanetary solar proton environments. The launch of the next SREM on Giove-B will provide further valuable measurements of the MEO environment and additional launches to the L-2 point will add to the solar proton and solar/interplanetary energetic electron measurements. This data is useful to studies of geomagnetic shielding, the drift of the south Atlantic anomaly, model validation and development, and the variability of signatures of energetic solar proton events.

The simple conversion factor for solar protons was shown to provide a reasonable flux calibration method that provides good agreement with the GOES measurements during the October 2003 event. Further comparisons of the variability of solar proton events with helio-longitude were presented.

The data from the INTEGRAL mission demonstrates the pessimism of the standard electron belt models above an L^* of 5 Earth radii and in particular at geostationary,

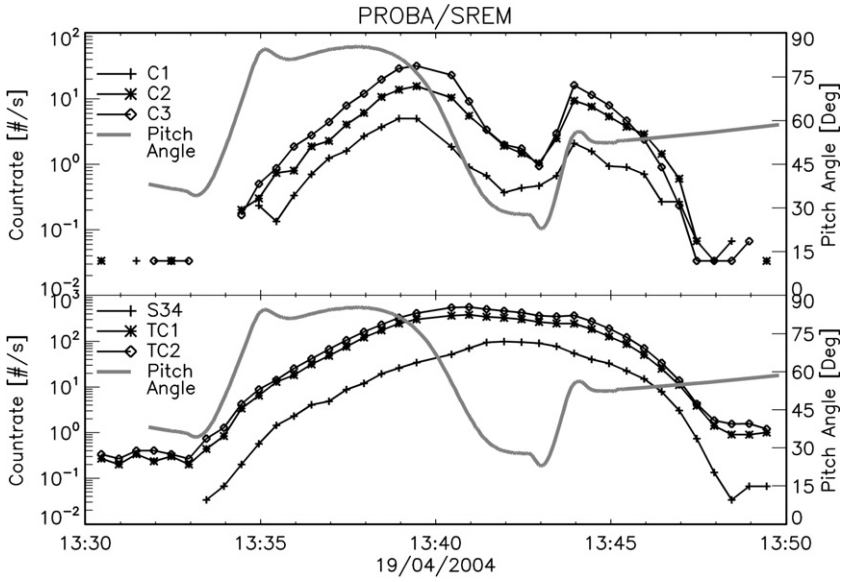

Fig. 18. The count rates from the coincident counters C1, C2, and C3 (upper panel) and the non-coincident counters S34, TC1 and TC2 channels (lower panel) during a single pass of the South Atlantic Anomaly with the pitch angle as derived from the on-board magnetometers.

but indicates that the models might be optimistic for L^* between 3 and 4.5 Earth radii. However, as the models present a long-term average, it will be necessary to revisit these comparisons as the datasets grow to cover more of the solar cycle and a greater sampling of the magnetosphere in this region is provided with the launch of Giove-B.

A comparison of the PROBA/SREM data with the proton belt models shows that these models generally overestimate. For the PROBA/SREM coincidence channels, though, more analysis of the effects of the pitch angle distribution on the count rate is required and a finer characterization of the small effect on the non-coincident counters.

References

Cain, J.C., Hendricks, S.J., Langel, R.A., Hudson, W.V. A proposed model for the international geomagnetic reference field, 1965. J. Geomag. Geoelectr. 19, 335, 1967.

Hajdas, W., Zehnder, A., Adams, L., Nickson, B. The proton irradiation facility at the Paul Scherrer Institut. Nucl. Instrum. Methods Phys. Res. B 113, 54, 1996.

INTEGRAL: Available from: <http://sci.esa.int/science-e/www/area/index.cfm?fareaid=21>.

Jensen, D.C., Cain, J.C. An interim geomagnetic field. J. Geophys. Res. 67, 3568, 1962.

NGDC/SPIDR: Available from: <http://spidr.ngdc.noaa.gov/spidr/>.

Olson, W.P., Pfitzer, K.A., Magnetospheric magnetic field modeling, Annual Scientific Report, AFOSR Contract No. F44620-75-C-0033, 1977.

ONERA/DESP: Boscher, D., Bourdarie, S., O'Brien, P., Guild, T., ONERA-DESP library V4.1. Available from: <http://craterre.onecert.fr/frames/category-menus.html>, 2004–2007.

PROBA: Available from: <http://www.esa.int/export/esaMI/Proba_web_site/>.

PSI/SREM: Available from: <http://srem.web.psi.ch/>.

ROSETTA: Available from: <http://sci.esa.int/science-e/www/area/index.cfm?fareaid=13>.

Vette, J.I., The NASA/National Space Science Data Center Trapped Radiation Environment Model Program (1964–1991), NSSDC/WDC-A-R& S 91-29, 1991.